# Structure and dynamics of the electronically excited C 1 and D 0# states of ArXe from high-resolution vacuum ultraviolet spectra

**Journal Article**

**Author(s):**
Piticco, Lorena; Schäfer, Martin; Merkt, Frédéric

**Publication date:**
2012-02-21

**Permanent link:**
https://doi.org/10.3929/ethz-a-010780812



**Originally published in:**
The Journal of Chemical Physics 136(7), https://doi.org/10.1063/1.3682770

**Funding acknowledgement:**
135342 - Rydberg states, VUV laser spectroscopy and photoionization dynamics (SNF)

The following article appeared in *J. Chem. Phys.* **136**, 074304(2012) and may be found at http://dx.doi.org/10.1063/1.3682770.

# Structure and dynamics of the electronically excited C 1 and D 0+ states of ArXe from high-resolution vacuum ultraviolet spectra

Lorena Piticco, Martin Schäfer, and Frédéric Merkt

Citation: The Journal of Chemical Physics **136**, 074304 (2012); doi: 10.1063/1.3682770
View online: http://dx.doi.org/10.1063/1.3682770
View Table of Contents: http://scitation.aip.org/content/aip/journal/jcp/136/7?ver=pdfcov
Published by the AIP Publishing



# Structure and dynamics of the electronically excited C 1 and D $0^+$ states of ArXe from high-resolution vacuum ultraviolet spectra

Lorena Piticco, Martin Schäfer, and Frédéric Merkt[a)]
*Laboratorium für Physikalische Chemie, ETH Zürich, 8093 Zürich, Switzerland*

(Received 9 December 2011; accepted 16 January 2012; published online 16 February 2012)

Vacuum ultraviolet spectra of the C 1 ← X $0^+$ and D $0^+$ ← X $0^+$ band systems of ArXe have been recorded at high resolution. Analysis of the rotational structure of the spectra of several isotopomers, and in the case of $Ar^{129}Xe$ and $Ar^{131}Xe$ also of the hyperfine structure, has led to the derivation of a complete set of spectroscopic parameters for the C 1 and D $0^+$ states. The rovibrational energy level structure of the C 1 state reveals strong homogeneous perturbations with neighboring $\Omega = 1$ electronic states. The analysis of isotopic shifts led to a reassignment of the vibrational structure of the C 1 state. The observation of electronically excited Xe fragments following excitation to the C state rotational levels of *f* parity indicates that the C state is predissociated by the electronic state of $0^-$ symmetry associated with the $Ar(^1S_0) + Xe(6s'[1/2]^o_0)$ dissociation limit. The observed predissociation dynamics differ both qualitatively and quantitatively from the behavior reported in previous investigations. An adiabatic two-state coupling model has been derived which accounts for the irregularities observed in the rovibronic and hyperfine level structure of the C 1 state. The model predicts the existence of a second state of $\Omega = 1$ symmetry, supporting several tunneling/predissociation resonances located ~200 $cm^{-1}$ above the C 1 state. © *2012 American Institute of Physics*. [http://dx.doi.org/10.1063/1.3682770]

## I. INTRODUCTION

Rare-gas dimers play an important role in chemical and physical processes taking place in the discharges of excimer lasers, in rare-gas ion lasers, and in high-pressure lamps.[1–6] Their electronic spectrum is complex:[7–11] Rydberg series converging on all six low-lying electronic states of the singly charged rare-gas dimer cations overlap spectrally and interact. Configurational mixing and spectral perturbations are extensive in the electronically excited states, and many states are predissociative and/or have potential-energy functions with multiple minima.[8,10,12–15]

Despite considerable progress in studies of the electronic structure and dynamics of rare-gas dimers since the first measurements of their vacuum ultraviolet electronic spectra,[16–23] the understanding of most band systems remains incomplete. Available predictions of the properties of electronically excited states by *ab initio* quantum chemistry[24–27] are not accurate enough to enable unambiguous spectral assignments.

The absence of g / u electronic symmetry in the heteronuclear rare-gas dimers leads to less restrictive optical and perturbation selection rules and to richer spectral structures than in the case of the homonuclear rare-gas dimers. At the same time it enables the observation of the same electronic states by single-photon (vacuum ultraviolet (VUV)) and non-resonant two-photon excitation from the weakly bound ground state. In the case of ArXe, which is the subject of the present article, information on many band systems has been obtained from single-photon VUV spectra[9,28–32] and resonance-enhanced multiphoton ionization spectra.[21,22,33–38] Several electronically excited states located in the vicinity of the $Ar(^1S_0) + Xe^*$ ($Xe^* = 6s[3/2]^o_2$, $6s[3/2]^o_1$, $6s'[1/2]^o_0$, $6s'[1/2]^o_1$, $6p[1/2]_1$, $6p[1/2]_0$, $6p[5/2]_2$, $6p[5/2]_3$, $6p[3/2]_1$, and $6p[3/2]_2$) dissociation limits have been assigned from direct observation of the rotational structure (see, e.g., Ref. 29), from the dependence of the observed intensity distributions on the polarization of the radiation used to record multiphoton excitation spectra (see, e.g., Ref. 36) or from photoelectron spectra recorded from selected excited states (see, e.g., Ref. 33).

The present article focuses on an investigation of the spectrum of ArXe in the vicinity of the $Ar(^1S_0) + Xe^*$ ($Xe^* = 6s'[1/2]^o_1$ and $6p[1/2]_1$) dissociation limits in the spectral region 77100–77250 $cm^{-1}$ by high-resolution VUV spectroscopy. In this spectral region two band systems, labelled C 1 ← X and D $0^+$ ← X in previous studies, overlap spectrally[9,28,29,32,36,38] and reveal pronounced perturbations and a rich predissociation dynamics. The high resolution achieved in our investigation enabled us to (i) precisely measure isotopic shifts and determine unambiguous vibrational assignments, (ii) fully resolve the rotational structure of most vibrational bands and obtain information on the potential-energy functions of the excited states and on perturbations, (iii) observe the hyperfine structure of the spectra of $Ar^{129}Xe$ and $Ar^{131}Xe$ and thus gain additional insight into the electronic structure, and (iv) derive an upper bound for the predissociation rates from the observed linewidths. The new information contained in our spectra enabled a better characterization of the C 1 and D $0^+$ states of ArXe, and the derivation of an adiabatic potential-energy function for the C 1 state on the basis of a two-state coupling model.

a)Electronic mail: merkt@xuv.phys.chem.ethz.ch.

 

## II. EXPERIMENTAL

The spectra of the D $0^+$, C $1 \leftarrow$ X $0^+$ transitions of ArXe have been recorded using a narrow bandwidth (full width at half maximum of 0.008 $cm^{-1}$) VUV laser system coupled to a time-of-flight (TOF) mass spectrometer described in Ref. 39. Only technical aspects relevant to the present investigation are summarized here.

Tunable VUV radiation in the range of $\tilde{\nu}_{VUV} = 77000–77350\ cm^{-1}$ was generated by resonance-enhanced, difference-frequency mixing ($\tilde{\nu}_{VUV} = 2\tilde{\nu}_{UV} - \tilde{\nu}_2$) in an atomic beam of krypton using two near-Fourier-transform-limited pulsed dye lasers. The laser pulses were produced by pulse amplifying the cw output of two single-mode ring dye lasers using chains of three dye amplification stages pumped by the second harmonic (wavelength $\lambda = 532$ nm) of a Nd:YAG laser and frequency doubled (tripled) in $\beta$-barium-borate crystals. The four-wave mixing process was resonantly enhanced at the two-photon level by locking the wave number $\tilde{\nu}_{UV} = 3\tilde{\nu}_1$ of the tripled output of the first dye laser to the position $2\tilde{\nu}_{UV} = 94092.906\ cm^{-1}$, which corresponds to the $4p^5\ (^2P_{3/2})\ 5p[1/2]_0 \leftarrow 4p^6\ ^1S_0$ two-photon resonance of atomic krypton. The locking was achieved by stabilizing the fundamental frequency of the dye laser to a selected hyperfine component of a transition of molecular iodine.[40]

The VUV wave number was tuned by scanning the wave number $\tilde{\nu}_2$ of the second pulsed dye laser. The wave number $\tilde{\nu}_2$ was calibrated by recording - with each VUV spectrum - several étalon spectra using étalons of different free spectral ranges and a laser-induced-fluorescence spectrum of $I_2$. The absolute VUV wave numbers could be calibrated with an accuracy of 0.02 $cm^{-1}$ and, with the étalon spectra, relative spectral positions could be determined with a precision of better than 0.002 $cm^{-1}$. The difference-frequency VUV beam was separated from the fundamental beams and beams generated in other nonlinear optical processes using a LiF prism and was directed towards the photoexcitation region where it intersected the probe gas beam at right angles.

The ArXe dimers were formed in a pulsed skimmed supersonic expansion of a 10:1 mixture of Ar and Xe held at a nozzle stagnation pressure of 2.5 bar. The skimmer opening (diameter 1 mm) was placed 3 cm away from the nozzle orifice and 6 cm away from the photoexcitation spot. The timing of the nozzle opening was set so as to maximize the ArXe dimer production and minimize the formation of $Ar_nXe_m$ clusters with $n, m > 1$. Ionization of the ArXe dimers after resonant VUV excitation was achieved by using the third harmonic (wavelength $\lambda = 355$ nm) of the same Nd:YAG laser that was used to pump the amplification stages. The ions were extracted by applying pulsed voltages on cylindrical metallic plates surrounding the photoexcitation region and detected at the end of the TOF tube using a microchannel plate (MCP) detector. The resolution of the TOF mass spectrometer was sufficient to fully separate the ion signals of different isotopomers. By setting adequate temporal gates in the TOF mass spectra and monitoring the ion signals in these gates as a function of the VUV wave number, spectra of the six dominant isotopomers of ArXe ($^{40}Ar^{129}Xe$ (natural abundance 26.3%), $^{40}Ar^{130}Xe$ (4.1%), $^{40}Ar^{131}Xe$ (21.1%), $^{40}Ar^{132}Xe$ (26.8%), $^{40}Ar^{134}Xe$ (10.4%), and $^{40}Ar^{136}Xe$ (8.8%) (Ref. 41)) were recorded simultaneously. The lasers used in the two-photon excitation sequence also enabled the detection of predissociation processes of the type ArXe* $\rightarrow$ Ar($^1S_0$) + Xe* with Xe* in the $6s'[1/2]^o_0$ state, because the third harmonic of the Nd:YAG laser efficiently ionized the excited Xe fragments.

## III. RESULTS AND DISCUSSION

Rotationally resolved (1 + 1′) resonance-enhanced two-photon ionization (R2PI) spectra of the D $0^+$ ($v' = 0 - 3$), C 1 ($v' = 0 - 6$) $\leftarrow$ X $0^+$ band systems of several isotopomers of ArXe were recorded at a resolution of 0.01 $cm^{-1}$ in the wave-number range from 77000 $cm^{-1}$ to 77300 $cm^{-1}$ corresponding to the overview, low-resolution spectrum displayed in Fig. 1. These band systems are presented in Subsections III A and III B, respectively. Subsection III C is devoted to the analysis of the hyperfine structure of the C 1 $\leftarrow$ X $0^+$ transitions of $^{40}Ar^{129}Xe$ and $^{40}Ar^{131}Xe$, and Subsection III D to a study of the perturbations and predissociation of the C 1 state.

### A. The D $0^+ \leftarrow$ X $0^+$ transition

Figure 2 displays the (1 + 1′) R2PI spectra of transitions from the X $0^+$ ground state to the lowest $v' = 0$ (panel a)), the $v' = 2$ (panel b)) and the $v' = 3$ (panel c)) vibrational levels of the D $0^+$ state of $^{40}Ar^{132}Xe$. The absence of a Q branch and the observation of the P(1) line in these spectra indicate that the transitions are parallel ($\Omega' = 0^+$) $\leftarrow$ ($\Omega'' = 0^+$) transitions, which confirms earlier assignments of this band system.[28,32,36] The strongly anharmonic nature of the potential-energy function of the weakly bound D $0^+$ state results in a significant change of the appearance of the P and R branches with increasing vibrational quantum number of the D state. At $v' = 0$, the P branch forms a band head at $J'' \cong 6$, indicating that the rotational constant is larger than in the ground state and that a contraction of the internuclear distance takes place upon excitation. In contrast, the $v' = 3$ band is characterized by a band head in the R branch at $J'' \cong 6$ indicating an elongation of the internuclear distance.

The rotational structures of the observed vibronic bands can be analyzed in terms of the standard expressions,

$$\tilde{\nu} = \tilde{\nu}_{v'v''} + (E'_{rot}(v', J') - E''_{rot}(v'', J''))/hc, \qquad (1)$$

and

$$\frac{E_{rot}(v, J)}{hc} = B_v J(J+1) - D_v J^2(J+1)^2 + H_v J^3(J+1)^3. \qquad (2)$$

A weighted least-squares fit of the observed VUV transition wave numbers together with the rotational transition frequencies of ArXe in the X $0^+$ ground state[42] yielded the molecular parameters summarized in Table I for the isotopomers $^{40}Ar^{129}Xe$, $^{40}Ar^{132}Xe$, and $^{40}Ar^{136}Xe$. These results indicate an equilibrium internuclear distance of the D $0^+$ state of about 3.76 Å, in agreement with the results of Refs. 28 and 32.

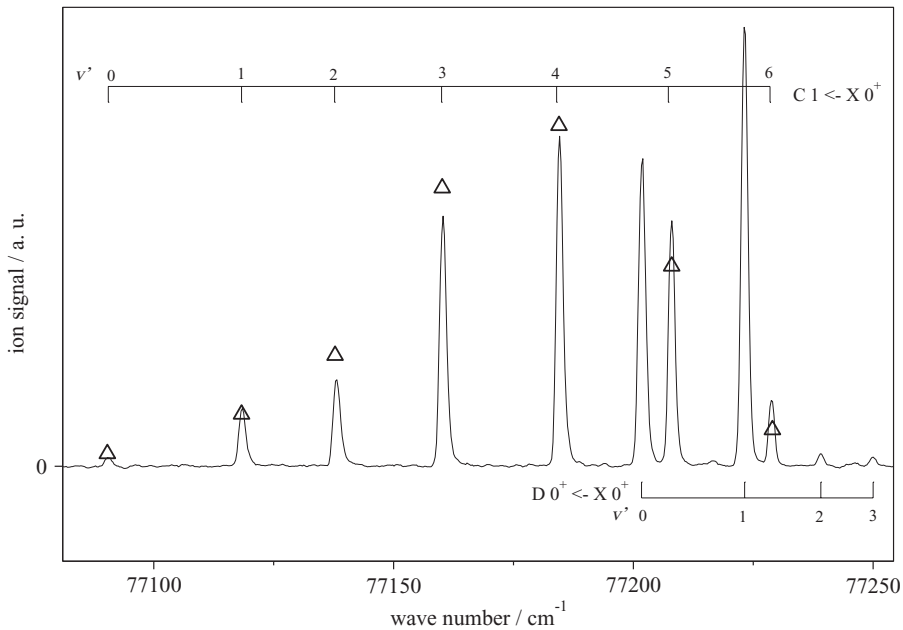


FIG. 1. Vibrationally resolved REMPI spectrum of the C 1 ($v' = 0 - 6$) ← X $0^+$ and D $0^+$ ($v' = 0 - 3$) ← X $0^+$ transitions of $^{40}Ar^{129}Xe$ in the vicinity of the $Xe^*(5p^5 6s'[1/2]_1^o) + Ar(^1S_0)$ dissociation limit (adapted from Ref. 32). The triangles indicate the calculated Franck–Condon factors of the C 1 ← X $0^+$ transitions.

A list of all transition wave numbers including experimental uncertainties is available as supplementary material.[43]

The experimental spectra of the D $0^+$ ($v'$) ← X ($v'' = 0$) transition (inverted traces) are compared in Fig. 2 with the calculated spectra obtained using the molecular parameters summarized in Table I, standard expressions for the Hönl-London factors,[44,45] and assuming a rotational temperature $T_{rot}$ = 3.5 K for ArXe in the supersonic beam. The overall agreement between calculated and measured spectra is good, and the observed deviations in the intensity distributions lie in the range of those expected from the intensity fluctuations of the VUV laser intensity and the fact that the population of the ground-state rotational levels may be only approximately described by a Boltzmann distribution. The analytical potential-energy function in Ref. 32 for the D $0^+$ state predicts the positions of the $v' = 0 - 3$ levels within 1 $cm^{-1}$ of the experimental results and no effort was invested to improve it. This good agreement confirms that the dissociation asymptote

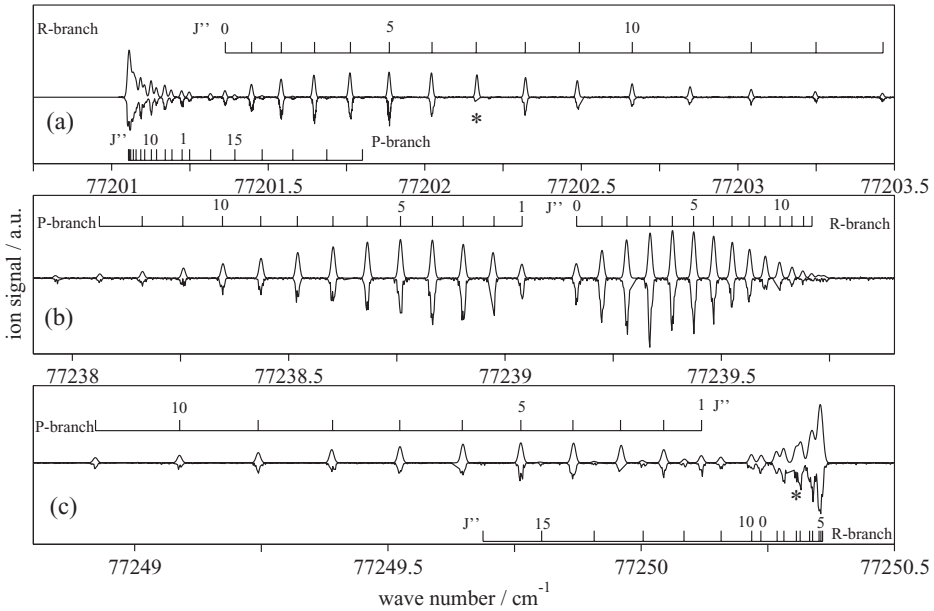


FIG. 2. Rotationally resolved spectra of the D $0^+$ ($v' = 0$) ← X $0^+$ (panel (a)), D $0^+$ ($v' = 2$) ← X $0^+$ (panel (b)), and D $0^+$ ($v' = 3$) ← X $0^+$ (panel (c)) transitions of $^{40}Ar^{132}Xe$. In each panel, the experimental spectra are shown as lower, inverted traces, and spectra calculated with the spectroscopic constants determined by a least-squares fit as upper traces. The assignment bars indicate the positions of the R($J''$) and P($J''$) transitions. The asterisks designate a region affected by a mode hop of the ring laser.

TABLE I. Band origins $\tilde{\nu}_{v'v''}$, rotational constants $B'_v$, $B''_v$, centrifugal distortion constants $D'_v$, $D''_v$, $H''_v$, and vibrational constants $\omega'_e$, $\omega_e x'_e$ for the D $0^+$ ($v'$) ← X $0^+$ ($v''$) transitions of $^{40}Ar^{129}$ Xe, $^{40}Ar^{132}$ Xe, and $^{40}Ar^{136}$ Xe. All values are in $cm^{-1}$. The least-squares fits gave a rms value of 0.8 in the case of $^{40}Ar^{129}$ Xe, 1.3 in the case of $^{40}Ar^{132}$ Xe, and 1.0 in the case of $^{40}Ar^{136}$ Xe. The values in parentheses represent one standard deviation in units of the last digit.

| Parameter | $^{40}Ar^{129}$ Xe | $^{40}Ar^{132}$ Xe | $^{40}Ar^{136}$ Xe |
|---|---|---|---|
| $\tilde{\nu}_{00}$ | 77201.27775(41)[a] | 77201.28758(38)[a]<br>77201.13[b] | 77201.30457(37)[a] |
| $\tilde{\nu}_{10}$ | 77223.022686(283)[a] | 77222.990709(272)[a]<br>77222.66[b] | 77222.949976(304)[a] |
| $\tilde{\nu}_{20}$ | 77239.14922(41)[a] | 77239.103024(314)[a]<br>77239.82[b] | 77239.04412(51)[a] |
| $\tilde{\nu}_{30}$ | 77250.22545(59)[a] | 77250.18275(47)[a]<br>77251.25[b] | 77250.12790(56)[a] |
| $B'_0$ | 0.0373656(60) | 0.0371643(53) | 0.03684380(245) |
| $D'_0/10^{-7}$ | 3.895(175) | 3.729(150) | |
| $B'_1$ | 0.03457589(257) | 0.03442117(235) | 0.0341671(37) |
| $D'_1/10^{-7}$ | 6.952(34) | 7.1476(261) | 6.476(72) |
| $B'_2$ | 0.0310034(128) | 0.0308756(49) | 0.0306793(180) |
| $D'_2/10^{-7}$ | 10.47(72) | 11.297(133) | 10.44(122) |
| $B'_3$ | 0.0272170(307) | 0.0270820(132) | 0.0269297(155) |
| $D'_3/10^{-7}$ | 8.58(219) | 8.91(68) | 10.08(71) |
| $B''_0$ | 0.032236849(8)<br>0.0322368493(17)[c] | 0.032065309(8)<br>0.03206530866(133)[c] | 0.031848134(12)<br>0.0318481341(26)[c] |
| $D''_0/10^{-7}$ | 2.24094(67)<br>2.24095(33)[c] | 2.21706(67)<br>2.21705(26)[c] | 2.18507(161)<br>2.18508(87)[c] |
| $H''_0/10^{-12}$ | − 6.411[d]<br>− 6.411(220)[c] | − 5.717[d]<br>− 5.717(170)[c] | − 6.538[d]<br>− 6.538(901)[c] |
| $\omega'_e$ | 27.0(3) | 26.9(3)<br>26.9(3)[b] | 26.8(2) |
| $\omega_e x'_e$ | 2.67(6) | 2.66(6)<br>2.56(6)[b] | 2.64(6) |

[a]Statistical uncertainty. The absolute uncertainty resulting from the calibration of VUV laser wave number is estimated to be ± 0.02 $cm^{-1}$ (see Sec. II).
[b]Values were taken from Ref. 28 and derived for a natural mixture of isotopomers.
[c]Values were taken from Ref. 42.
[d]Values were taken from Ref. 42 and kept constant during the fitting procedure.

of the D $0^+$ state corresponds to the Ar($^1S_0$) + Xe($6s'[1/2]^o_1$) fragments.

### B. The C 1 ← X $0^+$ transition

(1 + 1′) R2PI spectra of the C 1 ($v' = 0, 6$) ← X $0^+$ ($v'' = 0$) bands of $^{40}Ar^{132}$ Xe are depicted as inverted traces in Fig. 3, and are representative of the rotational structure observed for other bands of the C ← X transition. Each band consists of well-resolved P, Q, and R branches, with unambiguously observable R(0) and Q(1), but missing Q(0) transitions, as expected for a perpendicular ($\Omega' = 1$) ← ($\Omega'' = 0$) transition. The rotational structures of the C ($v'$) ← X (0) bands do not change as rapidly with $v'$ as in the case of the D ← X transition (compare with Fig. 2). This observation indicates that the attractive wall of the potential-energy function of the C 1 state is steeper than that of the D $0^+$ state. Given that the $v' = 5, 6$ levels of the C state are located in the same energy region as the $v' = 0 - 2$ levels of the D state, this observation suggests that the C 1 state correlates to a dissociation limit located above the dissociation limit of the D state, or that the C state potential-energy function has a barrier to dissociation. As will be shown in Secs. III C and III D, the analysis of the hyperfine structure of the $^{40}Ar^{129}$ Xe and $^{40}Ar^{131}$ Xe isotopomers suggests that the diabatic dissociation asymptote of the C 1 state corresponds to Ar($^1S_0$) and Xe($6p[1/2]_1$) fragments, which lies 84.104 $cm^{-1}$ above the dissociation limit of the D $0^+$ state, and not to Ar($^1S_0$) and Xe($6s'[1/2]^o_1$) as was assumed by Liu *et al.*[29] In their recent study of the C 1 state by (2 + 1) and (3 + 1) multiphoton excitation, Khodorkovskiĭ *et al.*[38] reached a similar conclusion, which is also supported by the calculations of Hickman *et al.*[26]

The analysis of the rotational structure of the C ← X $0^+$ transition of $^{40}Ar^{132}$ Xe was carried out using Eq. (1) in combination with Eq. (2) for the rotational structure of the X ground state and Eq. (3) for that of the C state ($\Omega = 1$),

$$\frac{E_{\rm rot}(v, J)}{hc} = B_v[J(J+1) - \Omega^2] - D_v[J(J+1) - \Omega^2]^2 + H_v[J(J+1) - \Omega^2]^3 \pm \frac{1}{2} q_v J(J+1). \quad (3)$$

In Eq. (3), $q_v$ represents the Ω-doubling constant, and the upper and lower signs of the Ω-doubling term (last term in Eq. (3)) correspond to the *e* and *f* parity levels, respectively.

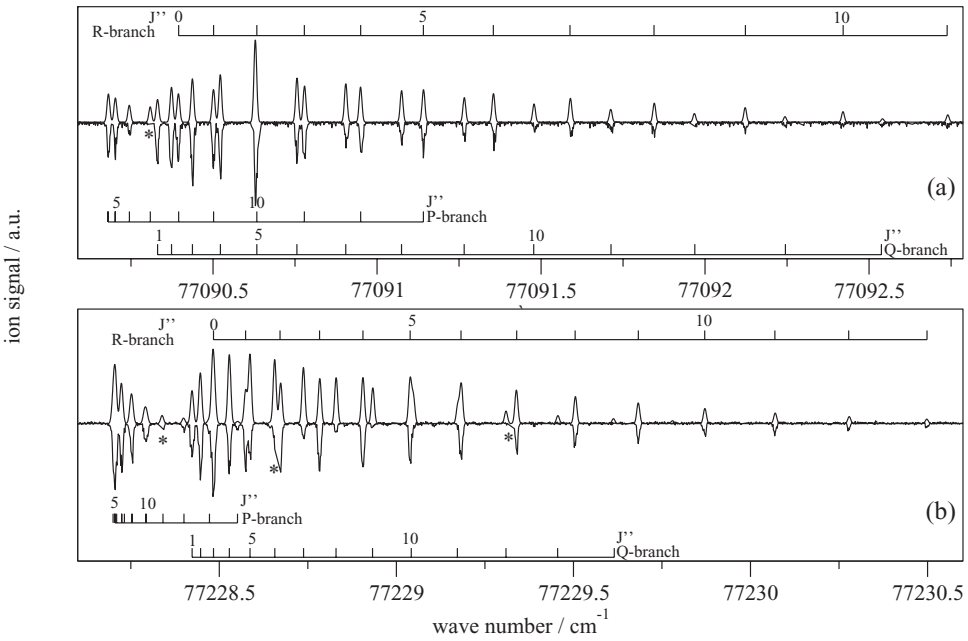


FIG. 3. High-resolution $(1 + 1')$ REMPI spectrum of the C 1 $(v' = 0) \leftarrow$ X $0^+$ $(v'' = 0)$ (upper panel) and C 1 $(v' = 6) \leftarrow$ X $0^+$ $(v'' = 0)$ (lower panel) transitions of $^{40}Ar^{132}$ Xe. The assignment bars indicate the positions of the P-, R-, and Q-branch transitions. The asterisks designate regions affected by mode hops of the ring laser.

Because all rotational levels of the X $0^+$ ground state have $e$ parity, P-, and R-branch transitions, which obey the selection rule $e \leftrightarrow e$ and $f \leftrightarrow f$, lead to the excitation of the upper ($e$) parity component of the Ω doublets. In the Hund's case (a) limit of a $^1\Pi$ state, this component would correspond to the $\Pi^+$ component. Q-branch transitions, which obey the selection rule $e \leftrightarrow f$, populate the lower ($f$) parity levels of the Ω doublets which correspond to the $\Pi^-$ component.

To obtain the band centers and the molecular constants $B'_v$, $D'_v$, $H'_v$, and $q'_v$ listed in the third column of Table II for $^{40}Ar^{132}$ Xe, the same procedure was followed as described in Sec. III A for the D $\leftarrow$ X transition.

The calculated spectra presented in Fig. 3 were obtained using standard expressions for the rotational line strengths[44,45] and assuming the same rotational temperature (3.5 K) as in the analysis of the D $\leftarrow$ X transition. High-$J$ states could only be observed for the $^{40}Ar^{132}$ Xe isotopomer. The Ω-doubling constant $q'_v$ of that isotopomer could therefore be determined precisely and was used to calculate the corresponding spectra of the other isotopomers. Comparing these results with those obtained previously at high resolution by Liu *et al.*[29] indicates several small, but significant discrepancies: (i) The band origins deviate by about 0.5 $cm^{-1}$, which may result from the fact that Liu *et al.*[29] calibrated their VUV frequency using transitions of the CO A-X band system whereas we used the procedure described in Sec. II; (ii) the values of the rotational constants obtained for the C state deviate significantly. The differences in the rotational constants arise because Liu *et al.*, although they also used the microwave data of Jäger *et al.*[42] in their analysis, converted MHz in $cm^{-1}$ by approximating the speed of light to $3.0 \times 10^{10}$ cm/s. In addition, they kept the value of the centrifugal distortion constants $D'_v$ fixed at the value of the vibronic ground state; (iii) the C-state vibrational quantum numbers in Refs. 28 and 29 differ from ours by +1 (see also Subsection III D); and (iv) the linewidths of the transitions observed in Ref. 29 were reported to be substantially larger than the bandwidth of 0.09 $cm^{-1}$ of the VUV laser used in the experiments, and the observed increase of the linewidth of Q-branch lines of the C-X band system with increasing rotational excitation was interpreted as resulting from predissociaton. In contrast, the linewidths observed in our study are limited by the instrumental resolution of $\simeq 0.015$ $cm^{-1}$, even in the case of the Q-branch lines of the C-X transitions.

Examination of the parameters listed for $^{40}Ar^{132}$ Xe and $^{40}Ar^{136}$ Xe in Table II and the spectra displayed in Fig. 3 reveals the following anomalies, already noticed and discussed in Ref. 29:

1. The vibrational spacings of the C ($v'$) levels are irregular.
2. The rotational and centrifugal distortion constants do not vary smoothly with $v'$.
3. The relative intensity of the Q-branch lines with respect to the P- and R-branch lines of most spectra decreases with increasing $J$ value, and Q-branch lines are difficult to observe beyond $J'' = 10$.

These anomalies indicate that the C 1 state of ArXe is perturbed. Because the hyperfine structure of the spectra of $^{40}Ar^{129}$ Xe and $^{40}Ar^{131}$ Xe provides additional information, the analysis of the spectra of these isotopomers is presented in Sec. III C before discussing possible origins for the perturbations in Sec. III D.

### C. The hyperfine structure of the C 1 ← X $0^+$ transitions

In the spectra of the C $\leftarrow$ X transitions of isotopomers containing $^{129}$Xe ($I = 1/2$) or $^{131}$Xe ($I = 3/2$), the rotational

TABLE II. Band origins $\tilde{\nu}_{v'v''}$, rotational constants $B'_v$, $B''_v$, centrifugal distortion constants $D'_v$, $D''_v$, $H''_v$, hyperfine constants $h'_{\Omega,v}$, and Ω-doubling constans $q'_v$ for the C 1 ($v'$) ← X $0^+$ ($v''$) transitions of $^{40}Ar^{129}$ Xe, $^{40}Ar^{131}$ Xe, $^{40}Ar^{132}$ Xe, and $^{40}Ar^{136}$ Xe. All values are in $cm^{-1}$. The least-squares fits gave a rms value of 0.76 in the case of $^{40}Ar^{136}$ Xe, and of 1.6 in all other cases. The values in parentheses represent one standard deviation in units of the last digit.

| | | | $^{40}Ar^{132}$ Xe | | |
|---|---|---|---|---|---|
| Parameter | $^{40}Ar^{129}$ Xe | $^{40}Ar^{131}$ Xe | This work | Literature | $^{40}Ar^{136}$ Xe |
| $\tilde{\nu}_{00}$ | 77090.35091(37)[a] | 77090.34898(34)[a] | 77090.35241(45)[a] | 77090.36[b] | 77090.35418(46)[a] |
| $\tilde{\nu}_{10}$ | 77118.103975(205)[a] | 77118.066339(299)[a] | 77118.05167(34)[a] | 77118.58(3)[c]<br>77118.60(6)[d] | 77117.98497(40)[a] |
| $\tilde{\nu}_{20}$ | 77137.446533(197)[a] | 77137.372253(288)[a] | 77137.33987(43)[a] | 77137.98(1)[c]<br>77137.98(1)[d] | 77137.20795(55)[a] |
| $\tilde{\nu}_{30}$ | 77159.64338(35)[a] | 77159.51613(44)[a] | 77159.456298(272)[a] | 77160.09(2)[c]<br>77160.07(1)[d] | 77159.21843(35)[a] |
| $\tilde{\nu}_{40}$ | 77184.04257(35)[a] | 77183.873970(262)[a] | 77183.79318(39)[a] | 77184.41(3)[c] | 77183.47557(47)[a] |
| $\tilde{\nu}_{50}$ | 77207.41315(43)[a] | 77207.21208(48)[a] | 77207.12159(42)[a] | 77207.68(4)[c]<br>77207.73(2)[d] | 77206.75020(54)[a] |
| $\tilde{\nu}_{60}$ | 77228.75792(68)[a] | 77228.54801(45)[a] | 77228.44911(51)[a] | | 77228.05592(57)[a] |
| $B'_0/10^{-2}$ | 4.29192(139) | 4.28132(77) | 4.27078(137) | | 4.23913(83) |
| $D'_0/10^{-7}$ | 2.18(99) | 4.52(34) | 2.36(80) | | |
| $B'_1/10^{-2}$ | 4.55199(57) | 4.53345(57) | 4.52185(64) | 4.825(5)[e]<br>4.827(4)[f] | 4.48910(181) |
| $D'_1/10^{-7}$ | 15.603(240) | 15.161(197) | 13.672(211) | | 11.83(139) |
| $B'_2/10^{-2}$ | 4.78338(65) | 4.77144(38) | 4.76007(87) | 4.728(4)[e]<br>4.733(3)[f] | 4.72364(217) |
| $D'_2/10^{-7}$ | 4.451(208) | 5.869(97) | 5.100(298) | | 3.63(158) |
| $B'_3/10^{-2}$ | 4.44160(82) | 4.42735(44) | 4.41904(41) | 4.445(1)[e]<br>4.441(2)[f] | 4.39221(36) |
| $D'_3/10^{-7}$ | − 0.286(200) | | − 0.256(120) | | |
| $B'_4/10^{-2}$ | 4.24288(51) | 4.22895(33) | 4.22290(41) | 4.241(7)[e] | 4.19719(68) |
| $D'_4/10^{-7}$ | 4.129(105) | 4.037(75) | 4.170(70) | | 4.806(180) |
| $B'_5/10^{-2}$ | 4.05464(73) | 4.04526(67) | 4.03478(48) | 3.953(4)[e]<br>3.949(4)[f] | 4.00495(106) |
| $D'_5/10^{-7}$ | 6.197(165) | 6.749(178) | 5.551(115) | | 4.21(46) |
| $H'_5/10^{-11}$ | | | − 7.86(74) | | − 13.2(43) |

TABLE II. (*Continued*.)

| Parameter | $^{40}Ar^{129}$ Xe | $^{40}Ar^{131}$ Xe | $^{40}Ar^{132}$ Xe | | $^{40}Ar^{136}$ Xe |
|---|---|---|---|---|---|
| | | | This work | Literature | |
| $B'_6/10^{-2}$ | 3.80559(192) | 3.79586(56) | 3.79024(106) | | 3.76485(139) |
| $D'_6/10^{-7}$ | 8.98(96) | 9.236(137) | 8.95(36) | | 8.71(61) |
| $B''_0/10^{-2}$ | 3.2236849(8) | 3.2121580(12) | 3.2065309(8) | | 3.1848134(12) |
| | 3.22368493(17)[g] | 3.21215796(3)[g] | 3.206530866(133)[g] | | 3.18481341(26)[g] |
| $D''_0/10^{-7}$ | 2.24094(67) | 2.22567(161) | 2.21706(67) | | 2.18507(161) |
| | 2.24095(33)[g] | 2.22564(13)[g] | 2.21705(26)[g] | | 2.18508(87)[g] |
| $H''_0/10^{-12}$ | − 6.411[h] | − 5.197[h] | − 5.717[h] | | − 6.538[h] |
| | − 6.411(220)[g] | − 5.197(100)[g] | − 5.717(170)[g] | | − 6.538(901)[g] |
| $h'_{\Omega,0}$ | − 0.05988(92) | 0.01775[i] | | | |
| $h'_{\Omega,1}$ | − 0.05345(59) | 0.01584[i] | | | |
| $h'_{\Omega,2}$ | − 0.05141(60) | 0.01524[i] | | | |
| $h'_{\Omega,3}$ | − 0.06183(117) | 0.01833[i] | | | |
| $h'_{\Omega,4}$ | − 0.06428(126) | 0.01905[i] | | | |
| $h'_{\Omega,5}$ | − 0.07433(145) | 0.02203[i] | | | |
| $h'_{\Omega,6}$ | − 0.08641(160) | 0.02562[i] | | | |
| $q'_0/10^{-5}$ | 2.86[j] | 2.86[j] | 2.86(58) | | 2.86[j] |
| $q'_1/10^{-5}$ | 1.62[j] | 1.62[j] | 1.62(37) | | 1.62[j] |
| $q'_2/10^{-5}$ | − 2.18[j] | − 2.18[j] | − 2.18(66) | | − 2.18[j] |
| $q'_3/10^{-5}$ | 0.96[j] | 0.96[j] | 0.96(37) | | 0.96[j] |
| $q'_4/10^{-5}$ | − 2.03[j] | − 2.03[j] | − 2.03(39) | | − 2.03[j] |
| $q'_5/10^{-5}$ | − 3.40[j] | − 3.40[j] | − 3.40(43) | | − 3.40[j] |
| $q'_6/10^{-5}$ | − 4.98[j] | − 4.98[j] | − 4.98(74) | | − 4.98[j] |

[a]Statistical uncertainty. The estimated absolute uncertainty would be $\pm$ 0.02 cm$^{-1}$.
[b]Values were taken from Ref. 28.
[c]Values were taken from Ref. 29 which were recorded on the ArXe$^+$ mass channel.
[d]Values were taken from Ref. 29 which were recorded on the Xe$^+$ mass channel. The C-state vibrational quantum numbers assigned in Refs. 28 and 29 differ from those determined here by +1 (see also Ref. 36).
[e]$B^e_{v'}$ values were taken from Ref. 29 which were recorded on the ArXe$^+$ mass channel.
[f]$B^f_{v'}$ values were taken from Ref. 29 which were recorded on the Xe$^+$ mass channel.
[g]Values were taken from Ref. 42.
[h]Values were taken from Ref. 42 and kept constant during the fitting procedure.
[i]Values were calculated using the relation $h'_{\Omega,v}\left(^{40}Ar^{131}\,Xe\right) = -h'_{\Omega,v}\left(^{40}Ar^{129}\,Xe\right)/3.37340$ (Refs. 49 and 59) and kept constant during the fitting procedure.
[j]Values adapted from $^{40}Ar^{132}$ Xe isotopomer and kept constant during the fitting procedure.

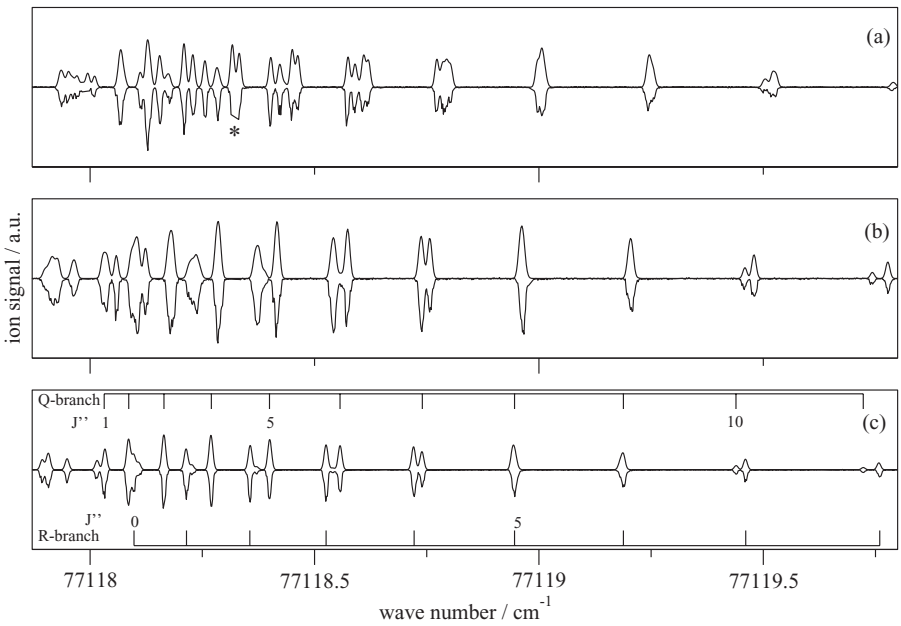


FIG. 4. Rotationally resolved spectra of the C 1 ($v' = 1$) ← X $0^+$ ($v'' = 0$) transitions of $^{40}Ar^{129}$ Xe (panel (a)), $^{40}Ar^{131}$ Xe (panel (b)), and $^{40}Ar^{132}$ Xe (panel (c)). In each panel, the experimental spectra are shown as lower, inverted traces, and the simulated spectra as upper traces. The asterisk designates a region affected by a mode hop of the ring laser.

transitions are split by the hyperfine interactions. The hyperfine structure is particularly pronounced in transitions involving low-$J''$ levels as illustrated in Fig. 4, where the spectra of the C 1 ($v = 1$) ← X $0^+$ ($v = 0$) transitions of $^{40}Ar^{129}Xe$ (top panel) and $^{40}Ar^{131}Xe$ (middle panel) are compared with that of $^{40}Ar^{132}Xe$ (bottom panel). The hyperfine structure is more prominent and better resolved in the spectrum of $^{40}Ar^{129}Xe$ for two reasons. First, the magnetic dipole moment of $^{129}Xe$ is about three times larger than that of $^{131}Xe$; second, the number of hyperfine components, which grows with the value of the nuclear spin quantum number $I$, is larger in the spectrum of $^{40}Ar^{131}Xe$, rendering the hyperfine structure more difficult to resolve.

To model the hyperfine structure that is observable in the C 1 ← X $0^+$ transition of $^{129}$XeAr and $^{131}$XeAr, the expression,[46,47]

$$\langle J\Omega I F|h_\Omega \vec{I}\cdot\vec{J}_a|J'\Omega I F\rangle = h_\Omega\,(-1)^{I+J'+F+J-\Omega}\times\begin{Bmatrix} I & J' & F \\ J & I & 1\end{Bmatrix}\begin{pmatrix} J & 1 & J' \\ -\Omega & 0 & \Omega\end{pmatrix} \times[I(I+1)(2I+1)]^{1/2}\,[(2J'+1)(2J+1)]^{1/2}\,\Omega \qquad (4)$$

was employed, with $\Omega = 1$ for the C state. The hyperfine coupling constant $h_\Omega$, defined as $a\Lambda + (b + c)\Sigma = a\Lambda + (b_F + \frac{2}{3}c)\Sigma$ in Hund's-coupling-case-(a) limit,[48] was used here as an effective coupling constant.

The relative intensity distributions of the C 1 ← X $0^+$ bands of $^{40}Ar^{129}Xe$ and $^{40}Ar^{131}Xe$ were calculated in the electric-dipole approximation using the expression,[46]

$$I(J'F' \leftarrow JF) \propto \left[\left\{(2J'+1)(2J+1)(2F'+1)(2F+1)\right\}^{1/2} \times\begin{pmatrix} 1 & J & J' \\ \Omega'-\Omega & \Omega & -\Omega'\end{pmatrix}\begin{Bmatrix} 1 & J & J' \\ I & F' & F\end{Bmatrix}\right]^2, \qquad (5)$$

which implies the selection rules $\Delta J = 0, \pm 1$ ($0 \not\leftrightarrow 0$) and $\Delta F = 0, \pm 1$ ($0 \not\leftrightarrow 0$) in addition to the parity selection rules mentioned above. The relative intensities of the transitions of $^{40}Ar^{132}Xe$ were calculated using the standard expressions for the Hönl-London factors.[44,45]

Because the hyperfine coupling in the spectrum of $^{40}Ar^{131}Xe$ could only be observed as a broadening of the rotational lines, no reliable values of $h_\Omega$ could be directly derived from the spectra. To model the hyperfine structure of this isotopomer, we assumed the ratio $h_\Omega(^{40}Ar^{129}Xe)$ / $h_\Omega(^{40}Ar^{131}Xe)$ to be identical to the ratio of the atomic hyperfine coupling constants $A(^{129}Xe)/A(^{131}Xe) = [\mu(^{129}Xe)/\mu(^{131}Xe)][I(^{131}Xe)/I(^{129}Xe)] = -3.373\,40(5)$,[49] and used the hyperfine coupling constant $h_\Omega(^{40}Ar^{129}Xe)$ to calculate that of $^{40}Ar^{131}Xe$. The excellent agreement between the calculated and experimental spectra in Fig. 4(b) confirms the validity of this assumption. The hyperfine coupling constants of the C 1 state of $Ar^{129}Xe$ determined from a weighted least-squares fit based on the line positions of the C-X band system and the rotational transitions reported by Jäger *et al.*[42] are summarized in the lower part of Table II.

In the limit where the argon atom is assumed not to interact significantly with the xenon atom, one would expect the

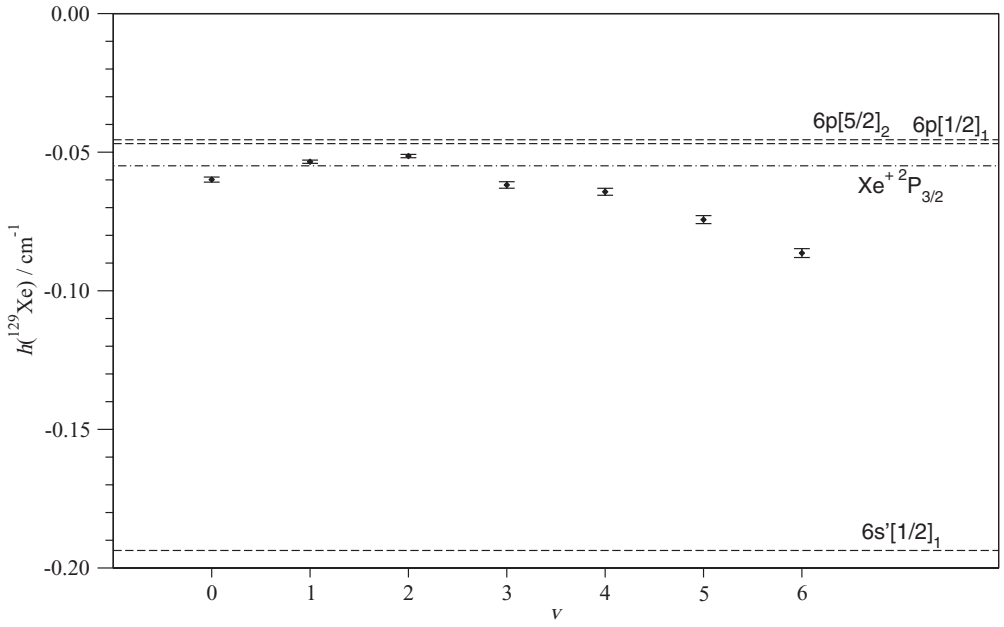


FIG. 5. Comparison of the $h_v$ hyperfine-coupling parameters of the C 1 ($v' = 0 - 6$) states of $^{40}$Ar$^{129}$ Xe with the corresponding magnetic-dipole hyperfine-coupling parameters of the relevant electronic states of Xe and Xe$^+$.[49,50,58]

hyperfine coupling constants to be $v$-independent and identical to the hyperfine coupling constant of the excited Xe atomic state at the dissociation limit of the C 1 potential curve. Our data, displayed in Fig. 5, indicate that $h_\Omega$ lies close to the hyperfine coupling constant of the Xe 6p[1/2]$_1$ ( $-$ 0.0469 cm$^{-1}$ (Ref. 50)), and 6p[5/2]$_2$ ( $-$ 0.0455 cm$^{-1}$ (Ref. 50)) levels up to $v = 4$. This observation supports the conclusion drawn in Sec. III B that the diabatic dissociation asymptote of the C state corresponds to Ar ($^1$S$_0$) and Xe (6p[1/2]$_1$) fragments. However, the hyperfine coupling constant decreases beyond $v = 4$. This trend will be discussed in Subsection III D 3.

### D. Perturbations and predissociation of the C 1 state

#### *1. Overall structure of the progression and vibrational assignment*

The irregular spectral patterns observed in the spectra of the C-X band system are reflected in irregular variations of the molecular parameters listed in Table II with the C-state vibrational quantum number. The evolution of the rotational constant $B_v$ and the centrifugal distortion constant $D_v$ of $^{40}$Ar$^{129}$Xe, $^{40}$Ar$^{131}$Xe, and $^{40}$Ar$^{132}$Xe are illustrated in panels a and b of Fig. 6. The Ω-doubling constant of $^{40}$Ar$^{132}$Xe and the hyperfine coupling constant $h_{\Omega,v}$ of $^{40}$Ar$^{129}$Xe are plotted in Figs. 6(c) and 6(d), respectively. Particularly striking is the increase by more than 10% of the value of $B_v$ between $v = 0$ and $v = 2$. In an unperturbed electronic state, this increase of $B_v$ with $v$ would imply that the attractive wall of the potential-energy function is steeper than the repulsive wall. However, the irregular vibrational spacings (see Fig. 6(e)) clearly indicate at least one perturbation.

We initially tried to rationalize the experimental observations by invoking two different vibrational progressions arising either from two different $\Omega = 1$ electronic states or from a double-minimum potential-energy function for the C 1 state. In either case, one would have expected the observed isotopic shifts to directly reveal the two different progressions. However, the observed isotopic shifts of the vibrational levels of all isotopomers were found to increase monotonically with excitation energy. The evolution of the isotopic shifts is illustrated in Fig. 6(f) in which the scaled isotopic shifts $\Delta\tilde{\nu}^i/(\rho_i - 1)$ of isotopomers $i$ ($i = {}^{40}$Ar$^{129}$Xe and $^{40}$Ar$^{131}$Xe),

$$\frac{\Delta\tilde{\nu}^i}{(\rho_i - 1)} = \frac{1}{hc}\frac{(E^i(v') - E^{\mathrm{ref}}(v'))}{(\rho_i - 1)}, \tag{6}$$

are plotted as a function of the vibrational quantum number. In Eq. (6), $E^i(v')$ represents the absolute energy (defined with respect to the minimum of the X 0$^+$ potential well[51]) of the vibrational level $v'$ of isotopomer $i$, $E^{\mathrm{ref}}(v')$ is the corresponding energy of the reference isotopomer, which was chosen to be $^{40}$Ar$^{132}$Xe, and $\rho_i = \sqrt{\frac{\mu_{\mathrm{ref}}}{\mu_i}}$, $\mu_i$ being the reduced mass of isotopomer $i$.

For a harmonic oscillator, the reduced isotopic shift

$$\frac{\Delta\tilde{\nu}^i}{(\rho_i - 1)} = \omega_e^{\mathrm{ref}} v + \frac{1}{2}\omega_e^{\mathrm{ref}} \tag{7}$$

is independent of the isotopomer and represents a linear function of $v$ with a slope of $\omega_e^{\mathrm{ref}}$ and an intercept of $\frac{1}{2}\omega_e^{\mathrm{ref}}$. The close-to-linear dependence of $\Delta\tilde{\nu}^i/(\rho_i - 1)$ on $v$ observed in Fig. 6(f) indicates that all $\Omega = 1$ levels observed experimentally are successive members of the same vibrational progression. The positive intercept of ~12 cm$^{-1}$ and the slope of

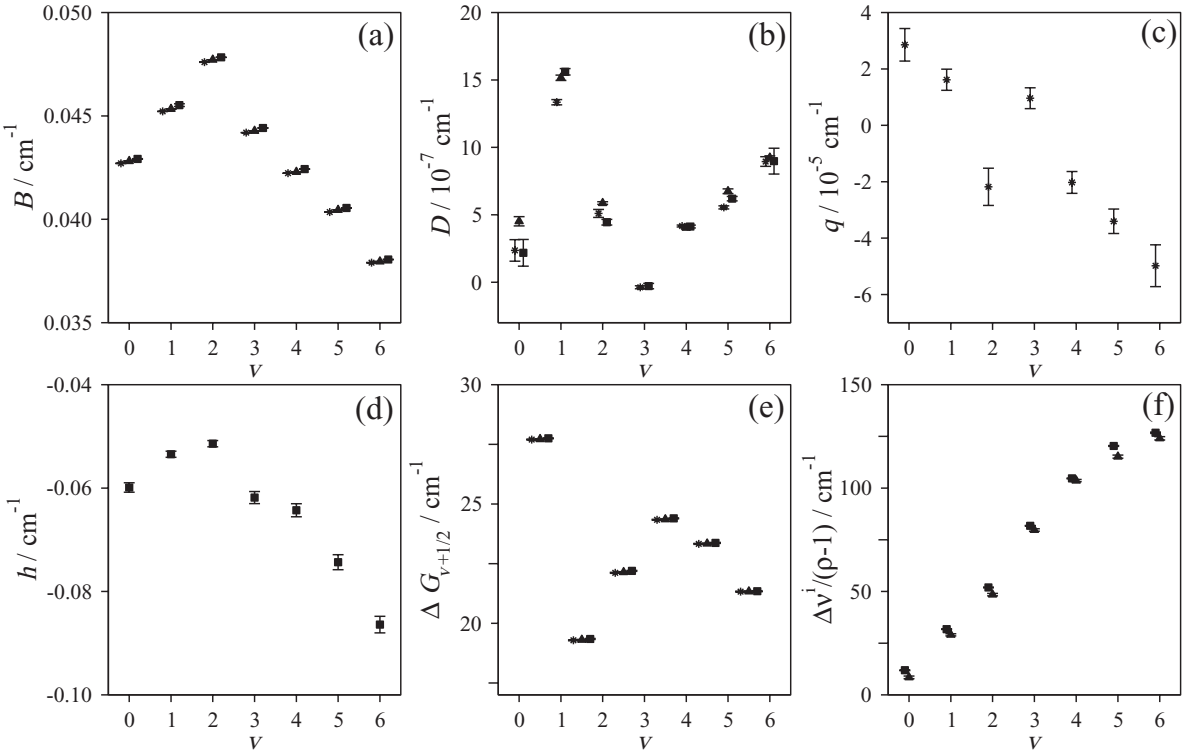


FIG. 6. Spectroscopic constants of the C 1 ($v' = 0 - 6$) ← X $0^+$ transitions of the $^{40}Ar^{129}Xe$ (squares), $^{40}Ar^{131}Xe$ (triangles), and $^{40}Ar^{132}Xe$ (stars) isotopomers. Upper part : (a) Rotational constants $B_v$, (b) centrifugal distortion constants $D_v$, and (c) Ω-doubling constants $q_v$. Lower part: (d) Hyperfine constants $h_v$ of $^{40}Ar^{129}Xe$, (e) vibrational intervals $\Delta G_{v+1/2}$ , and (f) scaled isotopic shifts of the band origins of $^{40}Ar^{129}Xe$ and $^{40}Ar^{131}Xe$ (corrected for the ground state isotope shifts, with $^{40}Ar^{132}Xe$ as reference isotopomer).

$\sim$25 cm$^{-1}$ further indicate that the lowest observed level is the $v = 0$ level of the C state. Using the vibrational assignment proposed by Tsuchizawa *et al.*[28] leads to a negative intercept of approximately −12 cm$^{-1}$. We therefore suspect that the very weak feature observed at 77069.3 cm$^{-1}$ in Ref. 28 (but not observed in later studies[29,32,36,38]) and assigned to the C-X (0,0) transition is not part of the C-X band system.

### 2. Predissociation of the C 1 state

In their study of the C 1 state of ArXe, Liu *et al.*[29] made three observations indicative of the predissociative nature of the C 1 state: (i) the observation of a $Xe^+$ signal arising from the ionization of excited Xe fragments with their ionization laser (wave number $\sim$23525 cm$^{-1}$). The spectra obtained by monitoring the $Xe^+$ signal were found to consist exclusively of Q-branch lines, which correspond to *f*-parity levels of the C state, whereas the spectra recorded by monitoring the $ArXe^+$ signal were found to be dominated by P- and R-branch lines corresponding to *e*-parity levels of the C state;[52] (ii) the observation of a broadening of the Q-branch lines increasing linearly with $J(J + 1)$; and (iii) the observation of a significant but *J*-independent broadening of the P- and R-branch lines.

Considering all relevant dissociation channels (see Table III) and taking into account the parity and *J* dependence of the linewidths and the fact that only Xe* fragments with internal energy above $\sim$74300 cm$^{-1}$ could be ionized with their laser of wave number of 23525 cm$^{-1}$, Liu *et al.*[29] drew the following conclusions:

1. The *f*-parity rotational levels of the C 1 state, which correspond to the $1^-$ component, must be predissociated by an $0^-$ electronic state (heterogeneous predissociation) which can only be the $0^-$ state associated with the $Ar(^1S_0) + Xe\ (6s'[1/2]^o_0)$ dissociation limit.
2. The *e*-parity rotational levels of the C state are subject to a homogeneous predissociation which leads to Xe fragments that cannot be ionized by their laser of wave number 23525 cm$^{-1}$. Consequently, the predissociation must be caused by one of the two $\Omega = 1$ levels associated with the $Ar(^1S_0) + Xe\ (6s'[3/2]^o_2)$ or the $Ar(^1S_0) + Xe\ (6s'[3/2]^o_1)$ dissociation limit.

As mentioned in Sec. III B, the linewidths of the transitions observed in the present study are limited by the instrumental resolution of 0.015 cm$^{-1}$ and are all much narrower than the bandwidth of 0.09 cm$^{-1}$ of the laser used in Ref. 29. Consequently, the line broadening observed by Liu *et al.* cannot be attributed to predissociation.

Figure 7 compares the $(1 + 1')$ R2PI spectrum of the C $1(v' = 2)$ ← X $0^+$ $(v'' = 0)$ transition of $^{40}Ar^{132}Xe$ (upper panel) with a spectrum recorded by monitoring the $Xe^+$ ions produced by the ionization of excited Xe* fragments (lower panel). Very similar results were obtained for the $v' = 0$–1 and 3–6 levels of the C state. The wave number of the ionization

TABLE III. Dissociation limits[60] and Hund's case (c) labels of the low-lying electronic states of ArXe and $ArXe^+$. The Rydberg-state character of the electronic states of ArXe is indicated in the last column. The positions are relative to the Ar ($^1S_0$) + Xe ($^1S_0$) limit, which lies 117 $cm^{-1}$ above the X $0^+$ ($v = 0$) ground state of ArXe.[51] All values are in $cm^{-1}$.

| Dissociation limit | Position | $\Omega$ | Ion core + Rydberg electron |
|---|---|---|---|
| $Ar^+\,^2P^o_{1/2}$ + Xe $^1S_0$ | 128 541.425 | $C_2$ 1/2 | |
| $Ar^+\,^2P^o_{3/2}$ + Xe $^1S_0$ | 127 109.842 | B 1/2, $C_1$ 3/2 | |
| Ar $^1S_0$ + $Xe^+\,^2P^o_{1/2}$ | 108 370.714 | $A_2$ 1/2 | |
| Ar $^1S_0$ + $Xe^+\,^2P^o_{3/2}$ | 97 833.790 | X 1/2, $A_1$ 3/2 | |
| Ar $^1S_0$ + Xe $6p[5/2]_2$ | 78 119.798 | 2, 1, $0^+$ | $(A_1\,3/2)\,6p\sigma$ |
| Ar $^1S_0$ + Xe $6p[1/2]_1$ | 77 269.144 | 1, $0^-$ | $(X\,1/2)\,6p\sigma$ |
| Ar $^1S_0$ + Xe $6s'[1/2]^o_1$ | 77 185.040 | 1, $0^+$ | $(A_2\,1/2)\,6s\sigma$ |
| Ar $^1S_0$ + Xe $6s'[1/2]^o_0$ | 76 196.767 | $0^-$ | |
| Ar $^1S_0$ + Xe $6s[3/2]^o_1$ | 68 045.156 | 1, $0^+$ | $(A_1\,3/2)\,6s\sigma$ |
| Ar $^1S_0$ + Xe $6s[3/2]^o_2$ | 67 067.547 | 2, 1, $0^-$ | $(X\,1/2)\,6s\sigma$ |
| Ar $^1S_0$ + Xe $^1S_0$ | 0.000 | X $0^+$ | |

laser used in our experiments (~28170 $cm^{-1}$) restricts the detection to the same fragments as in the study of Liu *et al.*[29] (see Table III). Although the relative intensities of P- and R-branch lines are similar in both spectra, the Q-branch lines are clearly depleted in the spectra recorded by detecting the $ArXe^+$ ions. This observation proves that the *f*-parity levels of the C state are predissociated by the $0^-$ electronic state associated with the Ar ($^1S_0$) + Xe ($6s'[1/2]^o_0$) dissociation limit which is located about 1000 $cm^{-1}$ below the region of interest (see Table III). The interaction between these two states also provides a possible explanation for the Ω doubling observed experimentally (see Subsection III B) although the $0^-$ level associated with the Ar($^1S_0$) + Xe*$6p[1/2]_1$ dissociation limit may also contribute to the perturbation. Interestingly, P- and R-branch lines are also observed in the spectra recorded by monitoring the $Xe^+$ signal (see Fig. 7(b)). However, one cannot conclude from this observation that the *e*-parity rotational levels of the C state are predissociative. Consideration of Table III leads to the conclusion that there are no $\Omega = 1$ levels with dissociation limits associated with Xe* fragments that can be detected with our ionization laser. Instead, we believe that the $Xe^+$ ions arise, in this case, from the dissociation of the $ArXe^+$ ions produced following absorption of the 355 nm radiation from the C state.

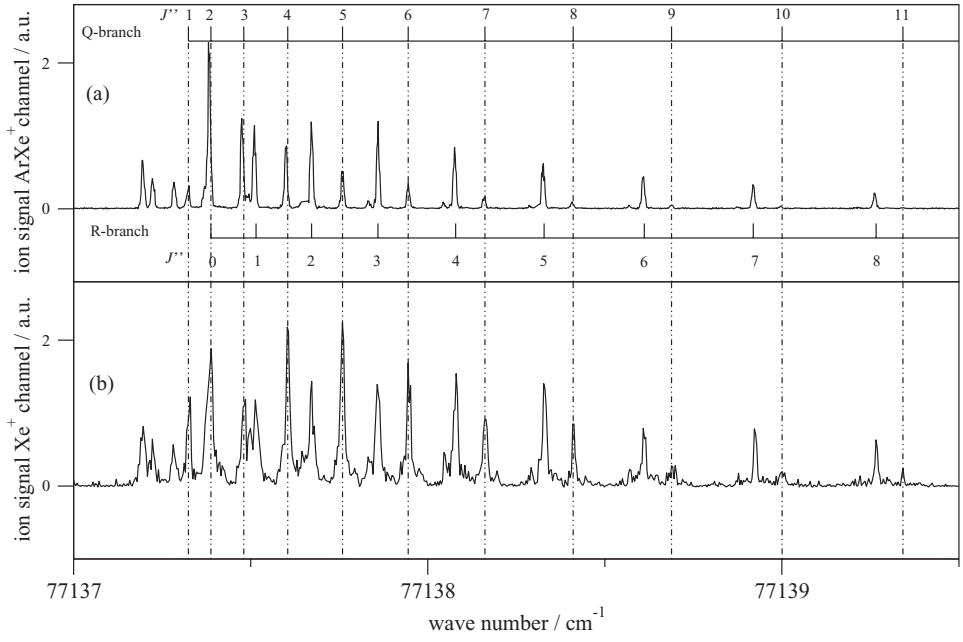


FIG. 7. Rotationally resolved spectra of the C 1 ($v' = 2$) ← X $0^+$ ($v'' = 0$) transition of $^{40}Ar^{132}Xe$ recorded in the mass channel of $^{40}Ar^{132}Xe^+$ (upper panel) and $^{132}Xe^+$ (lower panel). The positions of the Q-branch lines are indicated by vertical dashed-dotted lines to highlight the fact that their intensities in the $ArXe^+$ channel decrease much faster with increasing $J''$ value than the intensities of the R and P branches or of the Q branches in the $Xe^+$ channel, indicating that the C 1 (*f*) rovibrational levels decay by predissociation.

Our results on the predissociation of the C 1 state of ArXe thus differ qualitatively and quantitatively from those obtained by Liu *et al.*[29] We do not find any compelling evidence for a homogeneous predissociation mechanism. If this mechanism is at all operative, the corresponding rates must be much smaller than reported in Ref. 29. While our results confirm the existence of a heterogeneous predissociation involving the $\Omega = 0^-$ state associated with the Xe $(6s'[1/2]^o_0)$ + Ar $(^1S_0)$ asymptote, the narrow linewidth of all transitions observed in our study indicates that the predissociation rates are at least one order of magnitude slower than reported in Ref. 29. The rotational levels of the C state are therefore much longer lived than previously assumed, which makes these states ideally suited as intermediate levels in multiphoton excitation sequences.

### 3. Perturbation of the vibrational structure and potential model of the C state

The spectroscopic observations made on the C state of ArXe and presented in Secs. III D 1 and III D 2 indicate pronounced perturbations of the vibrational structure. Several explanations have been proposed to explain the irregular vibrational structure of the C state: From the discontinuity of the molecular parameters they observed around $v' = 4$ ($v' = 3$ according to the reassignment proposed in Sec. III D 1), Tsuchizawa *et al.*[28] inferred that the C state results from an avoided crossing between the repulsive $\Omega = 1$ state associated with the Ar $(^1S_0)$ + Xe $(6s[3/2]^o_1)$ limit (see Table III) and the bound state correlated with the Ar $(^1S_0)$ + Xe $(6s'[1/2]^o_1)$ limit (see Fig. 2 of Ref. 28 and Fig. 1 of Ref. 29). In this interpretation, the low vibrational levels with $v' \leq 3$ ($v' \leq 2$ according to our reassignment) of the C state are characteristic of the unperturbed bound state, whereas the properties of the levels with $v' \geq 4$ (3) reflect a state having an inner wall corresponding to the repulsive state. This interpretation cannot easily be reconciled with the observed increase of the rotational constant from $v' = 0$ to $v' = 2$ and with the fact that all observed levels, even those located closest to the proposed avoided crossing, are long lived. Moreover, the C state in the region of interest is likely to be correlated with the Ar $(^1S_0)$ + Xe $(6p[1/2]_1)$ dissociation limit, as explained in Subsection III B.

In their theoretical investigation of the low-lying Rydberg states of ArXe, Hickman *et al.*[26] noted that the three $\Omega = 1$ states associated with the Ar $(^1S_0)$ + Xe $(6s'[1/2]^o_1)$, Ar $(^1S_0)$ + Xe $(6p[1/2]_1)$, and Ar $(^1S_0)$ + Xe $(6p[5/2]_2)$ dissociation limits are strongly radially coupled and that the composition of the adiabatic states changes rapidly with $R$, and suggested that this phenomenon could account for the observation of Tsuchizawa *et al.*[28] Indeed, the mere fact that a transition is observed to the state correlating to the Ar $(^1S_0)$ + Xe $(6p[1/2]_1)$ limit, which is forbidden at long range in the electric-dipole approximation, suggests a mixing with the $\Omega = 1$ state associated with the Ar $(^1S_0)$ + Xe $(6s'[1/2]^o_1)$ state.

The spectroscopic data described in Subsection III B (see, in particular, Figs. 3 and 6 and Table II) provide the following additional information: (i) the rotational structures of all vibrational bands appear regular, as expected for a homogeneous perturbation with one or more $\Omega = 1$ states; (ii) all observed vibrational levels are part of the same vibrational progression, and the perturbation must be such that it leads to an increase of the rotational constant from $v' = 0$ to $v' = 2$; and (iii) the perturbing state cannot be particularly short-lived or repulsive, because one would otherwise have observed a reduction of the lifetimes of the most perturbed levels around $v' = 2$.

Table III contains a full list of the molecular states associated with the first dissociation limits of ArXe and $ArXe^+$. In the region of interest (77000–77250 $cm^{-1}$), three $\Omega = 1$ states correlating to the Ar$(^1S_0)$ + Xe$(6s'[1/2]^o_1)$, $(6p[1/2]_1)$, and $(6p[5/2]_2)$ dissociation limits must be considered. These states are low members of Rydberg series converging to the X 1/2, $A_1$ 3/2, and $A_2$ 1/2 states of the cation. Assuming that their potential-energy functions, in particular their dissociation energies and equilibrium internuclear distances, are similar to those of these ionic states (i.e., $D_0(X\ 1/2) = 1435.5\ cm^{-1}$, $R_e(X\ 1/2) = 3.154$ Å, $D_0(A_1\ 3/2) = 518.5\ cm^{-1}$, $R_e(A_1\ 3/2) = 3.711$ Å, $D_0(A_2\ 1/2) = 849.7\ cm^{-1}$, and $R_e(A_2\ 1/2) = 3.451$ Å (Ref. 32)), one can rule out contributions from the $(A_1\ 3/2)\ 6p\sigma$ state in combination with the Xe $(6p[5/2]_2)$ dissociation limit for energetical reasons. Moreover, the small values of the rotational constants of the C 1 state determined from the spectra (see Table II and Fig. 6(a)) are incompatible with a significant contribution from Rydberg states having an X 1/2 ion core. Consequently, only two $\Omega = 1$ molecular states, the $(A_1\ 3/2)\ 6p\sigma$ state associated with the $(6p[1/2]_1)$ limit and the $(A_2\ 1/2)\ 6s\sigma$ state associated with the $(6s'[1/2]^o_1)$ limit, were considered when modeling the potential-energy function of the C 1 state in the ranges of energy and internuclear distance relevant to the present investigation.

The spectroscopic observations could be interpreted using a model involving an interaction between these two states, described by the effective Hamiltonian

$$H = \begin{pmatrix} V^{\mathrm{d}}_{6s'}(R) & a_{\mathrm{s,p}}(R) \\ a_{\mathrm{s,p}}(R) & V^{\mathrm{d}}_{6\mathrm{p}}(R) \end{pmatrix}, \tag{8}$$

in which $V^{\mathrm{d}}_{6s'}(R)$ and $V^{\mathrm{d}}_{6\mathrm{p}}(R)$ represent the diabatic potential-energy functions of the $[A_1\ 3/2]$-core and $[A_2\ 1/2]$-core Rydberg states correlating with the Ar$(^1S_0)$ + Xe$(6s'[1/2]^o_1)$ and Ar$(^1S_0)$ + Xe$(6p[1/2]_1)$ dissociation limits, respectively, and $a_{\mathrm{s,p}}(R)$ describes the coupling between these two diabatic states. The $R$-dependent eigenvalues of Eq. (8) represent two adiabatic potential-energy functions of mixed 6s′ and 6p character, the lower of which corresponds to the C 1 state. The vibrational energy levels and corresponding rotational constants were determined numerically from these adiabatic potential-energy functions following the procedure described in Ref. 13.

The diabatic potential-energy functions $V^{\mathrm{d}}_{6s'}(R)$ and $V^{\mathrm{d}}_{6\mathrm{p}}(R)$ were described by functions of the general form[14]

$$V(R) = E_{\mathrm{Diss}} + V_{\mathrm{BM}}(R) + V_{\mathrm{Attr}}(R) + V_{\mathrm{Rep}}(R). \tag{9}$$

In Eq. (9), $E_{\mathrm{Diss}}$ corresponds to the position of the relevant dissociation limits relative to the X $0^+$ ($v = 0$) ground state of ArXe. $V_{\mathrm{BM}}(R) = Ae^{-bR}$ represents the Born–Mayer term describing the repulsive part of the potential functions at

TABLE IV. Diabatic potential parameters and switch function parameters $R_s$ and $W_s$ of the interacting $\Omega = 1$ Rydberg states correlating with the Ar ($^1S_0$) + Xe ($6s'[1/2]^o_1$) (indicated as $V_{6s'}(R)$) and Ar ($^1S_0$) + Xe ($6p[1/2]_1$) (indicated as $V_{6p}(R)$) dissociation limits. The numbers in brackets correspond to the standard deviations in units of the last digit. The root-mean-square deviation of the fit was determined to be rms = 30.

| Parameter | $V_{6s'}(R)$ | $V_{6p}(R)$ |
|---|---|---|
| $A$ (cm$^{-1}$) | $2.6 \times 10^7$ [a] | $3.8 \times 10^7$ [b] |
| $b$ (Å$^{-1}$) | 2.986(90) | 3.2 [b] |
| $C_{Attr}$ [c] (a.u.) | 6.02(162) | 1.37(2) |
| $C_{Rep}$ [d] (a.u.) | 0.190(50) | $6.49(108) \times 10^{-3}$ |
| $a^0_{s,p}$ (cm$^{-1}$) | | 143(20) |
| $R_s$ (Å) | | 5.25 |
| $W_s$ (Å) | | 0.7 |

[a]Estimated from the $A_2$ 1/2 ionic potential-energy curve determined in Ref. 32 and kept constant during the fitting procedure.
[b]Estimated from the $A_1$ 3/2 ionic potential-energy curve determined in Ref. 32 and kept constant during the fitting procedure.
[c]Atomic units: 1 a.u. $= a_0^2 E_h^2 e^{-4}$.
[d]Atomic units: 1 a.u. $= E_h a_0^2$.

short internuclear separations. $V_{Attr}(R) = -C_{Attr}\frac{Z(R)e^2\alpha}{R^4} f_4(R)$ describes the charge-induced-dipole interaction between the Ar ($^1S_0$) and the $Xe^+$ ion core in terms of the static polarizability $\alpha = 10.758 e^2 a_0^2 E_h^{-1}$ (Ref. 53) of Ar, the Tang-Toennies damping function $f_4(R) = 1 - e^{-bR}\Sigma_{k=0}^{4}\frac{(bR)^k}{k!}$,[54] and the effective charge $Z(R) = 1 - \int_0^R |\Psi_R(R)|^2 dR$ of the $Xe^+$ ion core. The last term in Eq. (9) represents the Pauli repulsion between the Rydberg electron and the electrons of the ground-state Ar atom and was calculated using[14]

$$V_{Rep}(R) = C_{Rep}\int_{R-r_{Ar}}^{R+r_{Ar}} \frac{|\Psi_R(R)|^2}{R^2} dR, \quad (10)$$

in which $\Psi_R(R)$ is the radial part of the Rydberg electron wave function given by[55]

$$\frac{\Psi_R(R)}{R} = K W_{\kappa,l+1/2}\left(\frac{2R}{\kappa}\right). \quad (11)$$

In Eq. (11), $K = [\kappa^2\Gamma(\kappa + l + 1)\Gamma(\kappa - l)]^{-1/2}$, $W_{\kappa,\mu}(z)$ is Whittaker's function[56] and $\kappa \equiv n^* = n - \delta$, where $\delta$ is the quantum defect. A value of $r_{Ar} = 1.5$ Å (Ref. 57) was used to evaluate Eq. (10).

Equation (9) offers the advantage that each diabatic potential-energy function is described by only four adjustable parameters ($A$, $b$, $C_{attr}$, and $C_{rep}$). These functions possess a hump originating from the Pauli repulsion.[8,12,14] The coupling term $a_{s,p}(R)$ must vanish at $R = \infty$ and was represented by the function,

$$a_{s,p}(R) = (1 - 0.5(1 + \tanh((R - R_s)/W_s)))a^0_{s,p}, \quad (12)$$

which is approximately constant at low $R$ values and decreases to zero in the range between $R_s - W_s$ and $R_s + W_s$, where $R_s$ and $W_s$ represent the center and the width of the switch function, respectively. In the calculations, $R_s$ and $W_s$ were kept fixed at the values $R_s = 5.25$ Å and $W_s = 0.7$ Å, respectively, so that the switch of the coupling constant from $a^0_{s,p}$ to 0 occurs outside the range of internuclear distances described by the experimental data. Initial values of the parameters $A$ and $b$ were obtained by fitting the first three terms of Eq. (9) to the known potential-energy functions of the $A_1$ 3/2 and $A_2$ 1/2 states of $ArXe^+$.[32] The nine parameters (one set of four parameters for each of the two diabatic potential functions and $a^0_{s,p}$) of the potential model were then determined from the observed positions and rotational constants of the C state vibrational levels in a least-squares fitting procedure. The results of the fit are presented in Table IV, which lists the optimal potential parameters, and Table V, which compares experimental and calculated values of the vibrational level positions and rotational constants.

The diabatic and adiabatic potential-energy functions are displayed in panels (a) and (b) of Fig. 8, respectively. The latter panel also displays the calculated vibrational wave functions corresponding to the levels observed experimentally. These functions and the known function of the $v = 0$ level of the X $0^+$ ground state of ArXe[51] resulted in the Franck–Condon factors displayed as triangles in Fig. 1.

The potential model provides a global description of the spectroscopic observations: the calculated positions of the vibrational bands agree within less than ~0.7 cm$^{-1}$ and the largest difference between the calculated and measured values of the rotational constants is ~0.001 cm$^{-1}$ (or 2% for $v = 1$). The unitless root-mean-square deviation of the fit is 30, primarily because the band centers and rotational constants have been determined experimentally with much higher precision than can be achieved with our model. Particularly satisfactory are the facts that (i) the potential model reproduces the increase of the rotational constants from $v' = 0$ to $v' = 2$ and its subsequent decrease at higher values of $v$, (ii) the calculated Franck–Condon factors correspond closely to the observed intensity distribution, and (iii) the increasing admixture of $6s'[1/2]^o_1$ character predicted for the C

TABLE V. Comparison of the experimental band origins $\tilde{\nu}_{exp}$ and rotational constants $B'_{exp}$ with the calculated band origins and rotational constants resulting from the adiabatic ($\tilde{\nu}^{ad}_{calc}$, $B^{ad}_{calc}$) treatment of the C 1 state of $^{40}Ar^{132}Xe$. All values are in cm$^{-1}$.

| $v'$ | 0 | 1 | 2 | 3 | 4 | 5 | 6 |
|---|---|---|---|---|---|---|---|
| $\tilde{\nu}_{exp}$ | 77090.35 | 77118.05 | 77137.34 | 77159.46 | 77183.79 | 77207.12 | 77228.45 |
| $\tilde{\nu}^{ad}_{calc}$ | 77089.90 | 77118.16 | 77137.11 | 77160.13 | 77184.37 | 77207.02 | 77227.84 |
| $\Delta\tilde{\nu}_{exp-calc}$ | 0.45 | −0.11 | 0.23 | −0.67 | −0.58 | 0.10 | 0.61 |
| $B'_{exp} \times (10^2)$ | 4.27 | 4.52 | 4.76 | 4.42 | 4.22 | 4.03 | 3.79 |
| $B^{ad}_{calc} \times (10^2)$ | 4.34 | 4.61 | 4.77 | 4.40 | 4.22 | 4.04 | 3.82 |
| $\Delta B_{exp-calc} \times (10^2)$ | −0.07 | −0.09 | −0.01 | 0.02 | 0.00 | −0.01 | −0.03 |

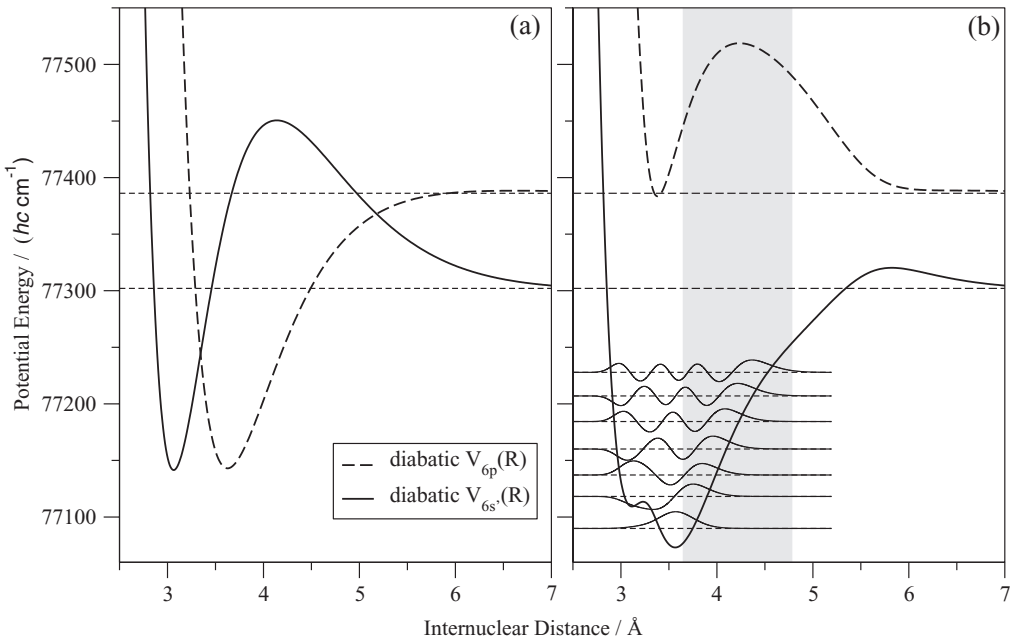


FIG. 8. Panel (a): Diabatic potential-energy functions of the $\Omega = 1$ states of ArXe correlating with the Ar ($^1S_0$) + Xe (6p[1/2]$_1$) (dashed line) and the Ar ($^1S_0$) + Xe (6s′[1/2]$^o_1$) (full line) dissociation limits of ArXe. The dashed horizontal lines correspond to the dissociation limits of these two states. Panel (b): Corresponding adiabatic potential-energy functions. The positions and wave functions of the observed vibrational levels of the C 1 state are drawn as dashed and full lines, respectively. The grey shaded area indicates the Franck–Condon region for excitation from the X $0^+$ ($v = 0$) ground state.

state vibrational levels beyond $v = 3$, which have vibrational wave functions extending toward the region where the two diabatic states are strongly mixed, provides a natural explanation for the gradual decrease of the hyperfine coupling constant observed for these levels (see Fig. 5).

Both diabatic potential-energy functions in Fig. 8(a) have a barrier to dissociation resulting from the Pauli repulsion between the Rydberg electron and the electrons of the closed-shell ground state argon atom. The barrier of the $\Omega = 1$ state correlating diabatically to the Ar ($^1S_0$) + Xe (6s′[1/2]$^o_1$) dissociation limit appears particularly pronounced. Such potential barriers are characteristic features of many excited electronic states of the rare-gas dimers.[8,12–15]

Although the potential-energy function of the lower adiabatic $\Omega = 1$ state in Fig. 8(b) should provide an accurate description of the C 1 state in the range of internuclear distances between 3 and 4.5 Å, where high-resolution spectroscopic data are available, it remains uncertain outside this range. The adiabatic potential-energy function of the upper $\Omega = 1$ state in Fig. 8(b) is even more uncertain and is expected to only provide a qualitative description of this state. No truly bound vibrational levels of this upper state are predicted by our potential model because all levels of the inner well are located above the Ar ($^1S_0$) + Xe (6p[1/2]$_1$) dissociation limit and can decay by tunneling. Moreover, the coupling to the continuum of the lower $\Omega = 1$ state is expected to result in rapid predissociation. We note that the Franck–Condon region (shaded area in Fig. 8(b)) would favour excitation of tunneling/predissociation resonances between 77400 and 77500 cm$^{-1}$. Such resonances lie in the range where broad spectral features have been observed in previous studies of the absorption spectrum[9,30] and the (3 + 1) resonance-enhanced multiphoton ionization (REMPI) spectrum[37] of ArXe. In particular, we believe that our potential model provides an attractive explanation for the broad resonance observed at ∼ 77400 cm$^{-1}$ in the (3 + 1) REMPI study.[37]

## IV. CONCLUSIONS

The combination of high-resolution VUV spectroscopy and mass spectrometry has enabled the recording of spectra of the C 1 ← X $0^+$ and D $0^+$ ← X $0^+$ band systems of ArXe which provide new information on the rovibrational energy level structure, on isotope shifts, on the hyperfine structure of $Ar^{129}Xe$ and $Ar^{131}Xe$, and on the predissociation dynamics of the C 1 and D $0^+$ states. Whereas the new data only enabled marginal improvement of the understanding of the D $0^+$ state of ArXe, it led to a new interpretation of the C 1 ← X $0^+$ band system, which includes a reassignment of the vibrational structure, the characterization of the heterogeneous perturbation causing the predissociation of the *f*-parity rotational levels and of the homogeneous perturbation responsible for the very irregular vibrational spacings of the C 1 state.

A two-state potential model was derived for the $\Omega = 1$ states of ArXe located in the vicinity of the Ar ($^1S_0$) + Xe (6s′[1/2]$^o_1$) and Ar ($^1S_0$) + Xe (6p[1/2]$_1$) dissociation limits which may prove useful when testing *ab initio* calculations of the electronically excited states of the rare-gas dimers and in the derivation of a global description of the electronic states of ArXe by multichannel quantum defect theory.

## ACKNOWLEDGMENTS

This work is supported financially by the Swiss National Science Foundation under Project No. 200020-135342 and by the European Research Council advanced grant program under Project No. 228286.

[1] *Excimer Lasers*, 2nd ed., Topics in Applied Physics Vol. 30, edited by Ch. K. Rhodes (Springer-Verlag, Berlin, 1984).
[2] *Vacuum Ultraviolet Spectroscopy*, edited by J. A.R. Samson and D. L. Ederer (Academic, San Diego, 2000).
[3] J. P. Boeuf, J. Phys. D **36**, R53 (2003).
[4] J. G. Eden, IEEE J. Sel. Top. Quantum Electron. **6**, 1051 (2000).
[5] J. J. Ewing, IEEE J. Sel. Top. Quantum Electron. **6**, 1061 (2000).
[6] D. A. Zayarnyi, L. V. Semenova, N. N. Ustinovskii, I. V. Kholin, and A. Yu. Chugunov, Quantum Electron. **27**, 957 (1997).
[7] M. L. Ginter and J. G. Eden, Can. J. Chem. **82**, 762 (2004).
[8] R. S. Mulliken, J. Chem. Phys. **52**, 5170 (1970).
[9] D. E. Freeman, K. Yoshino, and Y. Tanaka, J. Chem. Phys. **67**, 3462 (1977).
[10] C. D. Pibel, K. Yamanouchi, J. Miyawaki, S. Tsuchiya, B. Rajaram, and R. W. Field, J. Chem. Phys. **101**, 10242 (1994).
[11] P. M. Dehmer and S. T. Pratt, J. Chem. Phys. **88**, 4139 (1988).
[12] R. H. Lipson and R. W. Field, J. Chem. Phys. **110**, 10653 (1999).
[13] A. Wüest and F. Merkt, Chem. Phys. Lett. **397**, 344 (2004).
[14] E. Kleimenov, O. Zehnder, and F. Merkt, J. Mol. Spectrosc. **247**, 85 (2008), one should note that the factor $C_{\mathrm{Rep}}\sqrt{II^*}\frac{r^2}{4}$ in Eq. (9) of this article should be replaced by the factor $C_{\mathrm{Rep}}$ used in Eq. (10) of the present article.
[15] N. Y. Du and C. H. Greene, J. Chem. Phys. **90**, 6347 (1989).
[16] Y. Tanaka, K. Yoshino, and D. E. Freeman, J. Chem. Phys. **59**, 5160 (1973).
[17] D. E. Freeman, K. Yoshino, and Y. Tanaka, J. Chem. Phys. **71**, 1780 (1979).
[18] A. A. Madej and B. P. Stoicheff, Phys. Rev. A **38**, 3456 (1988).
[19] A. Balakrishnan, W. J. Jones, C. G. Mahajan, and B. P. Stoicheff, Chem. Phys. Lett. **155**, 43 (1989).
[20] M. J. Kiik, P. Dubé, and B. P. Stoicheff, J. Chem. Phys. **102**, 2351 (1995).
[21] D. M. Mao, X. K. Hu, Y. J. Shi, and R. H. Lipson, J. Chem. Phys. **111**, 2985 (1999).
[22] D. M. Mao, X. K. Hu, Y. J. Shi, and R. H. Lipson, Phys. Chem. Chem. Phys. **3**, 4258 (2001).
[23] R. H. Lipson, X. K. Hu, J. B.A. Mitchell, and C. Froese-Fischer, Phys. Rev. A **68**, 012717 (2003).
[24] P. Duplàa and F. Spiegelmann, J. Chem. Phys. **105**, 1492 (1996).
[25] C. Jonin and F. Spiegelmann, J. Chem. Phys. **117**, 3059 (2002).
[26] A. P. Hickman, D. L. Huestis, and R. P. Saxon, J. Chem. Phys. **96**, 2099 (1992).
[27] A. P. Hickman, D. L. Huestis, and R. P. Saxon, J. Chem. Phys. **98**, 5419 (1993).
[28] T. Tsuchizawa, K. Yamanouchi, and S. Tsuchiya, J. Chem. Phys. **92**, 1560 (1990).
[29] S. Liu, A. Hishikawa, and K. Yamanouchi, J. Chem. Phys. **108**, 5330 (1998).
[30] M. C. Castex, J. Chem. Phys. **66**, 3854 (1977).
[31] G. N. Gerasimov, B. E. Krylov, R. Hallin, A. O. Morozov, A. Arnesen, and F. Heijkenskjold, Opt. Spectrosc. **94**, 374 (2003).
[32] O. Zehnder and F. Merkt, J. Chem. Phys. **128**, 014306 (2008).
[33] S. T. Pratt, P. M. Dehmer, and J. L. Dehmer, J. Chem. Phys. **82**, 5758 (1985).
[34] S. T. Pratt, P. M. Dehmer, and J. L. Dehmer, J. Chem. Phys. **83**, 5380 (1985).
[35] S. S. Dimov, X. K. Hu, D. M. Mao, J. Y. Cai, and R. H. Lipson, J. Chem. Phys. **104**, 1213 (1996).
[36] D. M. Mao, X. K. Hu, S. S. Dimov, and R. H. Lipson, J. Phys. B **29**, L89 (1996).
[37] M. A. Khodorkovskiĭ, A. A. Belyaeva, L. P. Rakcheeva, P. Yu. Serdobintsev, A. A. Pastor, A. S. Mel'nikov, N. A. Timofeev, R. Hallin, and K. Siegbahn, Opt. Spectrosc. **104**, 674 (2008).
[38] M. A. Khodorkovskiĭ, S. V. Murashov, T. O. Artamonova, A. A. Beliaeva, L. P. Rakcheeva, A. A. Pastor, P. Yu. Serdobintsev, N. A. Timofeev, I. A. Shevkunov, I. A. Dement'ev, and J. Nordgren, J. Phys. B **43**, 155101 (2010).
[39] U. Hollenstein, H. Palm, and F. Merkt, Rev. Sci. Instrum. **71**, 4023 (2000).
[40] Th. A. Paul, J. Liu, and F. Merkt, Phys. Rev. A **79**, 022505 (2009).
[41] E. R. Cohen, T. Cvitaš, J. G. Frey, B. Holmström, K. Kuchitsu, R. Marquardt, I. Mills, F. Pavese, M. Quack, J. Stohner, H. L. Strauss, M. Takami, and A. J. Thor, *Quantities, Units and Symbols in Physical Chemistry*, 3rd ed. (RSC Publishing, Cambridge, England, 2007).
[42] W. Jäger, Y. Xu, and M. C. L. Gerry, J. Chem. Phys. **99**, 919 (1993).
[43] See supplementary material at http://dx.doi.org/10.1063/1.3682770 for the experimental and calculated positions of the transitions of the D $0^+ \leftarrow$ X $0^+$ and C $1 \leftarrow$ X $0^+$ band systems of all isotopomers investigated in the present work.
[44] G. Herzberg, *Molecular Spectra and Molecular Structure, Volume I, Spectra of Diatomic Molecules*, 2nd ed. (Van Nostrand Reinhold, New York, 1950).
[45] A. Hansson and J. K. G. Watson, J. Mol. Spectrosc. **233**, 169 (2005).
[46] K. J. Manke, T. R. Vervoort, K. T. Kuwata, and T. D. Varberg, J. Chem. Phys. **128**, 104302 (2008).
[47] J. M. Brown and A. Carrington, *Rotational Spectroscopy of Diatomic Molecules* (Cambridge University Press, Cambridge, England, 2003).
[48] R. A. Frosch and H. M. Foley, Phys. Rev. **88**, 1337 (1952).
[49] M. Schäfer, M. Raunhardt, and F. Merkt, Phys. Rev. A **81**, 032514 (2010).
[50] D. A. Jackson and M. C. Coulombe, Proc. R. Soc., London, Ser. A **335**, 127 (1973).
[51] L. Piticco, F. Merkt, A. A. Cholewinski, F. R.W. McCourt, and R. J. Le Roy, J. Mol. Spectrosc. **264**, 83 (2010).
[52] H. Lefebvre-Brion and R. W. Field, *Perturbations in the Spectra of Diatomic Molecules* (Academic, Orlando, 1986).
[53] J. Stiehler and J. Hinze, J. Phys. B **28**, 4055 (1995).
[54] K. T. Tang and J. P. Toennies, J. Chem. Phys. **80**, 3726 (1984).
[55] M. J. Seaton, Proc. Phys. Soc. London **88**, 801 (1966).
[56] M. Abramowitz and I. A. Stegun, eds., *Handbook of Mathematical Functions*, 9th ed. (Dover, London, 1970).
[57] Y. Zhang and Zh. Xu, Am. Mineral. **80**, 670 (1995).
[58] G. D'Amico, G. Pesce, and A. Sasso, Phys. Rev. A **60**, 4409 (1999).
[59] D. Brinkmann, Helv. Phys. Acta **41**, 367 (1968).
[60] J. E. Sansonetti and W. C. Martin, J. Phys. Chem. Ref. Data **34**, 1559 (2005).